Supporting Information

Beyond isotropic reorientation: Probing anisotropic and internal motions in ionic liquids with fast field cycling NMR relaxometry and MD simulations

Lennart Kruse,[a] Tanja van Alphen,[a] Johanna Busch,[a] Dietmar Paschek,[ab] Ralf Ludwig[abc] and Anne Strate*[a]

[a]*Physical and Theoretical Chemistry, Department of Chemistry, University of Rostock, Albert-Einstein-Str. 27, 18059 Rostock, Germany*

[b]*Department Life, Light and Matter, University of Rostock, Albert-Einstein-Str. 25, 18059 Rostock, Germany*

[c]*Leibniz Institute for Catalysis at the University of Rostock, Albert-Einstein-Str. 29a, 18059 Rostock, Germany*

*Corresponding author:
Anne Strate, Email: anne.strate@uni-rostock.de

Contents

S1 Relaxation theory

This section provides a comprehensive summary of all the equations employed in the models to fit the experimentally measured total spin-lattice relaxation rates of ^{1}H and ^{19}F nuclei. It includes the rate equations, the coupling parameters, and the spectral density functions, each of which plays a critical role in accurately describing the rotational and translational dynamics of the investigated ionic liquids (ILs).

Relaxation rates

$$\begin{aligned} R_1^{\mathrm{H}}(\omega_{\mathrm{H}}) &= R_{1,\mathrm{intra}}^{\mathrm{HH}}(\omega_{\mathrm{H}}) + R_{1,\mathrm{inter}}^{\mathrm{HH}}(\omega_{\mathrm{H}}) + R_{1,\mathrm{inter}}^{\mathrm{HF}}(\omega_{\mathrm{H}}) \\ &= A_{\mathrm{intra}}^{\mathrm{HH}} \times [J_{\mathrm{intra}}(\omega_{\mathrm{H}}) + 4J_{\mathrm{intra}}(2\omega_{\mathrm{H}})] \\ &+ A_{\mathrm{inter}}^{\mathrm{HH}} \times [J_{\mathrm{inter}}(\omega_{\mathrm{H}}) + 4J_{\mathrm{inter}}(2\omega_{\mathrm{H}})] \\ &+ A_{\mathrm{inter}}^{\mathrm{HF}} \times [J_{\mathrm{inter}}(|\omega_{\mathrm{H}} - \omega_{\mathrm{F}}|) + 3J_{\mathrm{inter}}(\omega_{\mathrm{H}}) + 6J_{\mathrm{inter}}(\omega_{\mathrm{H}} + \omega_{\mathrm{F}})] \end{aligned} \tag{1}$$

$$\begin{aligned} R_1^{\mathrm{F}}(\omega_{\mathrm{F}}) &= R_{1,\mathrm{intra}}^{\mathrm{FF}}(\omega_{\mathrm{F}}) + R_{1,\mathrm{inter}}^{\mathrm{FF}}(\omega_{\mathrm{F}}) + R_{1,\mathrm{inter}}^{\mathrm{FH}}(\omega_{\mathrm{F}}) \\ &= A_{\mathrm{intra}}^{\mathrm{FF}} \times [J_{\mathrm{intra}}(\omega_{\mathrm{F}}) + 4J_{\mathrm{intra}}(2\omega_{\mathrm{F}})] \\ &+ A_{\mathrm{inter}}^{\mathrm{FF}} \times [J_{\mathrm{inter}}(\omega_{\mathrm{F}}) + 4J_{\mathrm{inter}}(2\omega_{\mathrm{F}})] \\ &+ A_{\mathrm{inter}}^{\mathrm{FH}} \times [J_{\mathrm{inter}}(|\omega_{\mathrm{F}} - \omega_{\mathrm{H}}|) + 3J_{\mathrm{inter}}(\omega_{\mathrm{F}}) + 6J_{\mathrm{inter}}(\omega_{\mathrm{F}} + \omega_{\mathrm{H}})] \end{aligned} \tag{2}$$

Coupling constants

$$A_{\mathrm{intra}}^{\mathrm{HH}} = \frac{2}{5} I_{\mathrm{H}}(I_{\mathrm{H}}+1) \frac{1}{(r^{\mathrm{HH}})^6} \left[\frac{\mu_0}{4\pi}\gamma_{\mathrm{H}}^2\hbar\right]^2 \tag{3}$$

$$A_{\mathrm{inter}}^{\mathrm{HH}} = \frac{2}{5} I_{\mathrm{H}}(I_{\mathrm{H}}+1) N_{\mathrm{H}} \frac{4\pi}{3} \frac{1}{(d^{\mathrm{HH}})^3} \left[\frac{\mu_0}{4\pi}\gamma_{\mathrm{H}}^2\hbar\right]^2 \tag{4}$$

$$A_{\mathrm{intra}}^{\mathrm{FF}} = \frac{2}{5} I_{\mathrm{F}}(I_{\mathrm{F}}+1) \frac{1}{(r^{\mathrm{FF}})^6} \left[\frac{\mu_0}{4\pi}\gamma_{\mathrm{F}}^2\hbar\right]^2 \tag{5}$$

$$A_{\mathrm{inter}}^{\mathrm{FF}} = \frac{2}{5} I_{\mathrm{F}}(I_{\mathrm{F}}+1) N_{\mathrm{F}} \frac{4\pi}{3} \frac{1}{(d^{\mathrm{FF}})^3} \left[\frac{\mu_0}{4\pi}\gamma_{\mathrm{F}}^2\hbar\right]^2 \tag{6}$$

$$A_{\mathrm{inter}}^{\mathrm{HF}} = \frac{2}{15} I_{\mathrm{F}}(I_{\mathrm{F}}+1) N_{\mathrm{F}} \frac{4\pi}{3} \frac{1}{(d^{\mathrm{HF}})^3} \left[\frac{\mu_0}{4\pi}\gamma_{\mathrm{H}}\gamma_{\mathrm{F}}\hbar\right]^2 \tag{7}$$

$$A_{\mathrm{inter}}^{\mathrm{FH}} = \frac{2}{15} I_{\mathrm{H}}(I_{\mathrm{H}}+1) N_{\mathrm{H}} \frac{4\pi}{3} \frac{1}{(d^{\mathrm{FH}})^3} \left[\frac{\mu_0}{4\pi}\gamma_{\mathrm{F}}\gamma_{\mathrm{H}}\hbar\right]^2 \tag{8}$$

$$A_{\mathrm{inter}}^{\mathrm{HF}} \neq A_{\mathrm{inter}}^{\mathrm{FH}} \tag{9}$$

$$d^{\mathrm{HF}} = d^{\mathrm{FH}} \tag{10}$$

Spectral densities

The choice of the spectral density model for describing rotational dynamics is highly dependent on the geometry and rigidity of the ions. In contrast, translational dynamics are described using the same spectral density model for all ions.

Rigid spherical objects

As a first approximation, ions can be considered nearly spherical and rigid. Under these conditions, isotropic reorientation can be adequately described using a single Lorentzian function and a single rotational correlation time, following the BLOEMBERGEN-PURCELL-POUND (BPP) model[1]. The corresponding expressions are provided in Eqs. (11) and (12).

$$J_{\mathrm{intra}}^{\mathrm{BBP}}(\omega, \tau_{\mathrm{rot}}) = \frac{\tau_{\mathrm{rot}}}{1 + \omega^2 \tau_{\mathrm{rot}}^2} \tag{11}$$

$$\tau_{\mathrm{rot}} = \frac{1}{6 \cdot D_{\mathrm{rot}}} \tag{12}$$

Symmetric top

For rigid ions with a shape rather ellipsoidal than spherical, the symmetric top model[2,3] offers a more accurate representation of rotational reorientation. This model employs three Lorentzian functions to account for the anisotropic rotational dynamics, with the relevant expressions given in Eqs. (13) to (20).

$$\begin{aligned} J^{\mathrm{ST}}_{\mathrm{intra}} &= \frac{1}{4}(3\cos^2\alpha - 1)^2 \frac{6D_\perp}{(6D_\perp)^2 + \omega^2} \\ &+ 3(\sin^2\alpha\cos^2\alpha)\frac{5D_\perp + D_\parallel}{(5D_\perp + D_\parallel)^2 + \omega^2} \\ &+ \frac{3}{4}\sin^4\alpha \frac{2D_\perp + 4D_\parallel}{(2D_\perp + 4D_\parallel)^2 + \omega^2} \end{aligned} \tag{13}$$

$$\begin{aligned} J^{\mathrm{ST}}_{\mathrm{intra}} &= \frac{1}{4}(3\cos^2\alpha - 1)^2 \frac{\tau_0}{1 + \tau_0^2\omega^2} \\ &+ 3(\sin^2\alpha\cos^2\alpha)\frac{\tau_1}{1 + \tau_1^2\omega^2} \\ &+ \frac{3}{4}\sin^4\alpha \frac{\tau_2}{1 + \tau_2^2\omega^2} \end{aligned} \tag{14}$$

$$\frac{1}{\tau_m} = 6\,D_\perp + m^2(D_\parallel - D_\perp) \quad , \quad m = 0, 1, 2 \tag{15}$$

$$\frac{1}{\tau_0} = 6\,D_\perp = \frac{1}{\tau^{\mathrm{S}}_{\mathrm{rot}}} \tag{16}$$

$$\frac{1}{\tau_1} = 6\,D_\perp + (D_\parallel - D_\perp) = 5\,D_\perp + D_\parallel = \frac{1}{\tau^{\mathrm{S}}_{\mathrm{rot}}} + \frac{1}{\tau^{\mathrm{L}}_{\mathrm{rot}}} \tag{17}$$

$$\frac{1}{\tau_2} = 6\,D_\perp + 4\,(D_\parallel - D_\perp) = 2\,D_\perp + 4\,D_\parallel = \frac{1}{\tau^{\mathrm{S}}_{\mathrm{rot}}} + \frac{4}{\tau^{\mathrm{L}}_{\mathrm{rot}}} \tag{18}$$

$$\tau^{\mathrm{S}}_{\mathrm{rot}} = \frac{1}{6\,D_\perp} \tag{19}$$

$$\tau^{\mathrm{L}}_{\mathrm{rot}} = \frac{1}{D_\parallel - D_\perp} \tag{20}$$

Internal rotation

In cases where ions experience additional internal rotational motions beyond overall reorientation, a model describing isotropic rotational diffusion with one additional internal degree of freedom is required.[3–6] This approach also necessitates the use of three Lorentzian functions to capture the complexity of the motion and can be described by Eqs. (21) to (28).

$$J^{\mathrm{IR}}_{\mathrm{intra}} = \frac{1}{4}(3\cos^2\beta - 1)^2 \frac{6D}{(6D)^2 + \omega^2} + 3(\sin^2\beta\cos^2\beta)\frac{6D + D_{\mathrm{i}}}{(6D + D_{\mathrm{i}})^2 + \omega^2} + \frac{3}{4}\sin^4\beta\frac{6D + 4D_{\mathrm{i}}}{(6D + 4D_{\mathrm{i}})^2 + \omega^2} \tag{21}$$

$$J^{\mathrm{IR}}_{\mathrm{intra}} = \frac{1}{4}(3\cos^2\beta - 1)^2 \frac{\tau_0}{1 + \tau_0^2\omega^2} + 3(\sin^2\beta\cos^2\beta)\frac{\tau_1}{1 + \tau_1^2\omega^2} + \frac{3}{4}\sin^4\beta\frac{\tau_2}{1 + \tau_2^2\omega^2} \tag{22}$$

$$\frac{1}{\tau_m} = 6\,D + m^2 D_{\mathrm{i}} \quad , \quad m = 0, 1, 2 \tag{23}$$

$$\frac{1}{\tau_0} = 6\,D = \frac{1}{\tau_{\mathrm{rot}}} \tag{24}$$

$$\frac{1}{\tau_1} = 6\,D + D_{\mathrm{i}} = \frac{1}{\tau_{\mathrm{rot}}} + \frac{1}{\tau^{\mathrm{i}}_{\mathrm{rot}}} \tag{25}$$

$$\frac{1}{\tau_2} = 6\,D + 4\,D_{\mathrm{i}} = \frac{1}{\tau_{\mathrm{rot}}} + \frac{4}{\tau^{\mathrm{i}}_{\mathrm{rot}}} \tag{26}$$

$$\tau_{\mathrm{rot}} = \frac{1}{6\,D} \tag{27}$$

$$\tau^{\mathrm{i}}_{\mathrm{rot}} = \frac{1}{D_{\mathrm{i}}} \tag{28}$$

In all scenarios, the rotational dynamics can be characterized using both rotational correlation times τ and rotational diffusion coefficients D, providing a comprehensive description of the ion's behavior.

Force free hard sphere model

For a force free diffusion with a uniform distribution of the ions, and under the assumption of the reflecting wall boundary condition the spectral density for translational motion is given by Eq. (29)[7].

$$J_{\mathrm{inter}}(\omega, \tau_{\mathrm{trans}}) = 72\frac{3}{4\pi}\int_0^\infty \frac{u^2}{81 + 9u^2 - 2u^4 + u^6}\frac{u^2\tau_{\mathrm{trans}}}{u^4 + \omega^2\tau_{\mathrm{trans}}^2}\, du \tag{29}$$

$$\tau_{\mathrm{trans}}^{\mathrm{HF}} = \tau_{\mathrm{trans}}^{\mathrm{FH}} \tag{30}$$

This equation applies to the ^{1}H-^{1}H and the ^{19}F-^{19}F interactions, as well as the ^{1}H-^{19}F and ^{19}F-^{1}H interactions. As a result, it yields four distinct translational correlation times ($\tau_{\mathrm{trans}}^{\mathrm{HH}}$, $\tau_{\mathrm{trans}}^{\mathrm{FF}}$, $\tau_{\mathrm{trans}}^{\mathrm{HF}}$, $\tau_{\mathrm{trans}}^{\mathrm{FH}}$), of which only three are independent due to the constraint given by Eq. (30).
Translational correlation times can be used to calculate the relative diffusion coefficients $D_{\mathrm{rel}}(\mathrm{HH})$, $D_{\mathrm{rel}}(\mathrm{FF})$, and $D_{\mathrm{rel}}(\mathrm{HF})$ as well as self-diffusion coefficients of cations D_{H} and anions D_{F} according to Eqs. (31) and (33).

$$\tau_{\mathrm{trans}}^{\mathrm{HH}} = \frac{d_{\mathrm{HH}}^2}{D_{\mathrm{H}} + D_{\mathrm{H}}} = \frac{d_{\mathrm{HH}}^2}{2D_{\mathrm{H}}} = \frac{d_{\mathrm{HH}}^2}{D_{\mathrm{rel}}(\mathrm{HH})} \tag{31}$$

$$\tau_{\mathrm{trans}}^{\mathrm{FF}} = \frac{d_{\mathrm{FF}}^2}{D_{\mathrm{F}} + D_{\mathrm{F}}} = \frac{d_{\mathrm{FF}}^2}{2D_{\mathrm{F}}} = \frac{d_{\mathrm{FF}}^2}{D_{\mathrm{rel}}(\mathrm{FF})} \tag{32}$$

$$\tau_{\mathrm{trans}}^{\mathrm{HF}} = \frac{d_{\mathrm{HF}}^2}{D_{\mathrm{H}} + D_{\mathrm{F}}} = \frac{d_{\mathrm{HF}}^2}{D_{\mathrm{rel}}(\mathrm{HF})} \tag{33}$$

S2 Density information

For the calculation of temperature-dependent spin densities, we utilized previously published, experimentally measured macroscopic densities.[8] The spin density, N_I, can be determined from the fitted density using the following equation:

$$N_I = \frac{\rho \cdot N_{\mathrm{A}} \cdot n_I}{M} \tag{34}$$

where I denotes the corresponding nucleus, ρ is the macroscopic density, N_{A} is Avogadro's constant, n_I represents the number of respective nuclei per molecule or ion pair, and M is the molar mass.

Table S1: Fitted macroscopic densities and calculated spin densities of protons (N_{H}) and fluorines (N_{F}) in [TEA][NTf_2] and [C_5Py][NTf_2].

	[TEA][NTf_2]			[C_5Py][NTf_2]		
T / K	ρ_{fit} / g cm^{-3}	N_{H} / 10^{28} m^{-3}	N_{F} / 10^{28} m^{-3}	ρ_{fit} / g cm^{-3}	N_{H} / 10^{28} m^{-3}	N_{F} / 10^{28} m^{-3}
263	1.4636	3.6884	1.3832	1.4463	3.2381	1.1705
273	1.4538	3.6638	1.3739	1.4373	3.2178	1.1632
283	1.4441	3.6392	1.3647	1.4282	3.1974	1.1558
293	1.4343	3.6146	1.3555	1.4191	3.1771	1.1485
303	1.4246	3.5900	1.3463	1.4100	3.1567	1.1411
313	1.4148	3.5654	1.3370	1.4009	3.1364	1.1338
323	1.4051	3.5409	1.3278	1.3918	3.1160	1.1264
333	1.3953	3.5163	1.3186	-	-	-

S3 Viscosity information

The dynamic viscosities, η, of the pure ionic liquids were measured over the temperature range of 293–343 K using a microviscometer (Lovis 2000 ME, Anton Paar, Austria) based on the rolling ball principle. The estimated measurement accuracy for the viscosity data was $\pm$ 0.5 %.

Table S2: Experimentally obtained viscosities for [TEA][NTf_2] and [C_5Py][NTf_2].

	[TEA][NTf_2]	[C_5Py][NTf_2]
T / K	η / mPa s	η / mPa s
293	60.81	79.42
298	48.82	61.97
303	39.78	49.10
308	32.84	39.68
313	27.44	32.49
318	23.25	26.98
323	19.93	22.66
328	17.27	19.23
333	15.08	16.49
338	13.28	14.27
343	11.78	12.45

S4 Data fitting procedure

For the evaluation and fitting of the FFC data, we utilized a Matlab-based software, which has been developed in cooperation with Dr. Henning Schröder, earlier part of the faculty of Mathematics at the University of Rostock. The least-squares optimization was performed using the *lsqnonlin* function along with the *trust-region-reflective* algorithm. All datasets, including ^{1}H and ^{19}F spin-lattice relaxation data across all temperatures, were optimized simultaneously. To ensure an effective optimization process, certain constraints are applied, based on fundamental physical principles. The constraints that have been used during the fitting procedure are as follows:

- τ_{HH} decreases with increasing temperature
- τ_{HF} decreases with increasing temperature
- τ_{FF} decreases with increasing temperature

In contrast to the fitting parameters τ_{rot} and τ_{trans}, which are considered to be temperature-dependent, the structural parameters are expected to be temperature-independent. These structural parameters are the *distance-of-closest-approach*, d, and the intramolecular coupling constant, A_{intra}. The latter can be used to calculate the effective distance, r, between two coupling spins within the same molecule according to Eqs. (3) and (5). The obtained values for the temperature-independent parameters are presented in table S3.

Table S3: Optimized values of fitting parameters: d, being the *distance-of-closest-approach*, and r, representing the effective distance between two spins coupling intramolecularly.

	[TEA][NTf_2]	[C_5Py][NTf_2]
d_{HH} / Å	3.03	3.05
d_{FF} / Å	4.63	4.51
d_{HF} / Å	3.03	3.45
r_{HH} / Å	2.00	1.99
r_{FF} / Å	2.32	2.03

S5 Rotational correlation times

In the fitting procedure, the temperature behavior of the rotational correlation times was assumed to follow the VOGEL-FULCHER-TAMANN (VFT) equation (eq. (35)).

$$\tau_{rot} = \tau_{rot,0} \cdot \exp\left(\frac{B}{T - T_0}\right) \tag{35}$$

First, the three fitting parameters $\tau_{rot,0}$, B and T_0 are used with appropriate starting values. During the fit procedure, the parameter T_0 for the rotational dynamic of the $[TEA]^+$ cation in [TEA][NTf_2] decreased to a value being 5 magnitudes smaller than the actual temperature T. Therefore this parameter has been set to 0 and equation (35) simplifies to the well-known ARRHENIUS-equation. The obtained fitting parameters can be found in table S4. The temperature-dependent rotational correlation times are then calculated for each temperature from the fitted VFT-parameters following equation (35). The corresponding values are shown in tables S5 and S6.

Table S4: Fit Parameters of the rotational correlation times according to equation (35).

	[TEA][NTf_2]			[C_5Py][NTf_2]			
	$\tau_{rot,H}$	$\tau_{rot,F}$	$\tau^{i}_{rot,F}$	$\tau^{S}_{rot,H}$	$\tau^{L}_{rot,H}$	$\tau_{rot,F}$	$\tau^{i}_{rot,F}$
$\tau_{rot,0}$ / s	3.10×10^{-15}	2.03×10^{-13}	1.18×10^{-13}	6.36×10^{-13}	1.11×10^{-13}	3.34×10^{-13}	2.50×10^{-13}
B / K	3209.45	1262.85	948.50	1196.77	923.44	859.50	775.88
T_0 / K	0	111.00	137.94	134.36	156.10	170.90	145.72

Table S5: Experimental overall rotational correlation times for cations and anions in [TEA][NTf_2] including the rotational correlation time for the internal motion $\tau^{i}_{rot,F}$ in the $[NTf_2]^-$ anion.

	$[TEA]^+$	$[NTf_2]^-$	
T / K	$\tau_{rot,H}$ / ps	$\tau_{rot,F}$ / ps	$\tau^{i}_{rot,F}$ / ps
263.15	613.74	815.99	229.64
273.15	392.71	489.08	131.13
283.15	259.33	311.10	80.90
293.15	176.17	207.97	53.11
303.15	122.77	144.98	36.69
313.15	87.55	104.74	26.43
323.15	63.76	78.02	19.73
333.15	47.32	59.68	15.18

Table S6: Experimental rotational correlation times for cations and anions in [TEA][NTf_2] including the anisotropy of the $[C_5Py]^+$ cation and the rotational correlation time for the internal motion $\tau^{i}_{rot,F}$ in the $[NTf_2]^-$ anion.

	$[C_5Py]^+$		$[NTf_2]^-$	
T / K	$\tau^{S}_{rot,H}$ / ps	$\tau^{L}_{rot,H}$ / ps	$\tau_{rot,F}$ / ps	$\tau^{i}_{rot,F}$ / ps
263.15	6909.00	620.55	3715.66	185.12
273.15	3536.95	296.97	1493.42	110.22
283.15	1981.21	159.60	706.25	70.77
293.15	1193.81	93.91	377.52	48.25
303.15	763.85	59.39	221.85	34.54
313.15	513.78	39.82	140.49	25.73
323.15	360.40	28.00	94.47	19.82

From MD simulations we have calculated the reorientational correlation times as described in section 3 of the main article. This enables us to investigate the dynamics of certain molecular vectors, which can be compared to the rotational correlation times we obtained from the global fit of the FFC data. We have done this for selected molecular vectors and the corresponding reorientational correlation times for both ionic liquids can be found in tables S7 and S8. Here, a solid line between two nuclei represents a vector along a chemical bond and dots represent a molecular vector through space between the two nuclei. The indices o, m and p indicate the *ortho*, *meta* and *para* carbon atoms of the pyridinium ring.

Table S7: Reorientational correlation times $\tau_{X\text{-}Y}$ for different molecular vectors within the $[TEA]^+$ cation and the $[NTf_2]^-$ anion in the IL [TEA][NTf_2] obtained from molecular dynamics simulations. An asterisk indicates results from MD simulations using a time step of 1 fs and system sizes of $N = 256$ ion pairs.

	T/ K	$\tau_{N\text{-}H}$/ ps	$\tau_{N\text{-}C}$/ ps	$\tau_{C\text{-}C}$/ ps		
$[TEA]^+$	250	2550	969	630		
	250*	2748	1043	726		
	280	487	197	135		
	300	243	96.1	65.9		
	340	77.2	33.6	23.7		
	380	35.9	15.8	11.1		
	380*	35.4	15.8	11.4		
	T/ K	$\tau_{C\ldots C}$ / ps	$\tau_{F\ldots F,\,long}$ / ps	$\tau_{F\ldots F,\,short}$ / ps	$\tau_{C\text{-}F}$ / ps	$\tau_{S\text{-}O}$ / ps
$[NTf_2]^-$	250	2530	1900	370	180	1010
	250*	2773	2075	381	196	1148
	280	401	312	73.3	50.1	171
	300	183	144	37.6	28.4	80.1
	340	55.9	44.4	14.2	12.0	27.0
	380	25.3	20.4	7.18	6.33	12.3
	380*	24.9	20.4	7.65	6.91	12.7

Table S8: Reorientational correlation times $\tau_{X\text{-}Y}$ for different molecular vectors within the $[C_5Py]^+$ cation and the $[NTf_2]^-$ anion in the IL $[C_5Py][NTf_2]$ obtained from molecular dynamics simulations.

	T/ K	$\tau_{Cp\ldots C5}$/ ps	$\tau_{Cp\ldots N}$/ ps	$\tau_{Co\text{-}Cm}$/ ps	$\tau_{C2\text{-}C3}$/ ps	$\tau_{C4\text{-}C5}$/ ps
$[C_5Py]^+$	300	549	281	278	99.4	44.6
	320	263	137	135	53.1	23.5
	340	146	76.5	75.6	32.0	14.5
	360	89.0	48.0	47.4	21.5	9.63
	380	59.5	32.4	32.0	15.3	6.88
	400	42.1	23.2	22.9	11.4	5.11
	T/ K	$\tau_{C\ldots C}$ / ps	$\tau_{F\ldots F,\,long}$ / ps	$\tau_{F\ldots F,\,short}$ / ps	$\tau_{C\text{-}F}$ / ps	$\tau_{S\text{-}O}$ / ps
$[NTf_2]^-$	300	214	159	34.0	27.0	74.84
	320	103	77.5	18.6	16.3	36.30
	340	57.4	44.2	11.4	10.7	20.89
	360	35.8	27.6	7.80	7.56	13.44
	380	24.3	18.9	5.68	5.71	9.37
	400	17.5	13.7	4.36	4.26	6.91

S6 Self-diffusion coefficients

The experimental self-diffusion coefficients are calculated according to equations (31) - (33), with the translational correlation time τ_{trans} and the *distance of closest approach* d being fit parameters. The self-diffusion coefficients from MD simulations are calculated following the procedure described in the main text of this paper (section 3). Table S10 shows the experimental as well as the simulated self-diffusion coefficients of both ionic liquids. Additionally, the experimental obtained self-diffusion coefficients are fitted according to the VOGEL-FULCHER-TAMANN equation. The general equation is

$$D = D_0 \cdot \exp\left(-\frac{B}{T - T_0}\right) \tag{36}$$

and the corresponding fit parameters can be found in table S9.

Table S9: Fit Parameters of the self-diffusion coefficients according to equation (36).

	[TEA][NTf_2]		[C_5Py][NTf_2]	
	D_{H}	D_{F}	D_{H}	D_{F}
D_0 / $\mathrm{m^2\,s^{-1}}$	3.90×10^{-9}	2.02×10^{-8}	1.12×10^{-9}	2.40×10^{-10}
B / K	558.82	1024.21	428.38	228.00
T_0 / K	183.27	150.20	196.29	224.08

Table S10: Experimental and simulated self-diffusion coefficients for cations D_{H} and anions D_{F} in [TEA][NTf_2] and [C_5Py][NTf_2]. An asterisk indicates results from MD simulations using a time step of 1 fs and system sizes of $N = 256$ ion pairs.

		[TEA][NTf_2]		[C_5Py][NTf_2]	
	T / K	D_{H} / $10^{-12}\,\mathrm{m^2\,s^{-1}}$	D_{F} / $10^{-12}\,\mathrm{m^2\,s^{-1}}$	D_{H} / $10^{-12}\,\mathrm{m^2\,s^{-1}}$	D_{F} / $10^{-12}\,\mathrm{m^2\,s^{-1}}$
experimental	263.15	4.287	2.042	1.647	1.279
	273.15	9.480	5.311	4.582	2.427
	283.15	13.710	10.577	8.560	4.758
	293.15	22.779	13.632	12.938	8.837
	303.15	35.918	23.704	19.460	12.311
	313.15	53.317	40.490	30.166	20.497
	323.15	73.863	52.515	37.838	23.231
	333.15	92.483	74.924	-	-
simulation	250	1.82	1.65	-	-
	250*	1.77	1.54	-	-
	280	12.2	10.7	-	-
	300	27.1	23.6	17.5	14.7
	320	-	-	40.1	31.5
	340	93.8	79.6	76.8	60.8
	360	-	-	122	100
	380	204	182	183	159
	380*	204	162	-	-
	400	-	-	259	195

S7 Molecular Dynamics Simulations

Classical molecular dynamics (MD) simulations were performed using non-polarizable unscaled force fields for the $[NTf_2]^-$ anion[9,10], the $[TEA]^+$ cation[11,12], and the $[C_5Py]^+$ cation[13]. Simulations were conducted under constant pressure and temperature (NpT) conditions at a pressure of 1 bar. All MD simulations were executed using the GROMACS 5.0.6[14–18] simulation package. Initial simulation boxes were created by arranging the ions on an interpenetrating primitive cubic lattice. The systems were then initially equilibrated for 2 ns at 500 K employing the BERENDSEN thermostat and barostat[19] with coupling times of $\tau_{\mathrm{T}} = \tau_{\mathrm{p}} = 0.5\,\mathrm{ps}$. The systems were then equilibrated again for 2 ns following a sequence of decreasing temperatures. After equilibration, production runs with simulation length t_{sim} given in Tables S11 and S12 were carried out, employing the NOSÉ-HOOVER (NH) thermostat[20,21] (no NH chain) and the PARRINELLO-RAHMAN barostat[22,23] with coupling times of $\tau_{\mathrm{T}} = 1\,\mathrm{ps}$ and $\tau_{\mathrm{p}} = 2\,\mathrm{ps}$ respectively. Here, we have followed the recommendations given by Basconi and Shirts[24], who found that the application of the Nosé-Hoover thermostat yield reliable dynamical properties that are statistically indistinguishable from those of the microcanonical (NVE) ensemble, given that it is applied globally. All simulations were performed with a 2 fs time step employing periodic boundary conditions. For comparison, additional simulations with a shorter time-step of 1 fs were also performed. Constraints to ensure fixed bond-lengths were solved using the LINCS algorithm[25]. All bond length were kept fixed during the simulation. The smooth particle mesh EWALD summation[26] was applied in the liquid with a mesh spacing of $0.12\,\mathrm{nm}$, a real space cutoff of $0.9\,\mathrm{nm}$ and 4th order interpolation. The relative accuracy of the EWALD sum was set to 10^{-5} corresponding to a convergence factor $\alpha = 3.38\,\mathrm{nm^{-1}}$.

Table S11: Parameters characterizing the performed MD simulations of [TEA][NTf_2]. t_{sim}: total simulation time; N_{IP}: number of ion pairs; ρ: mass density. An asterisk indicates results from MD simulations using a time step of 1 fs

.

T/K	t_{sim}/ns	N_{IP}	ρ/kg m^{-3}
250	500	256	1464.6
250*	500	256	1465.9
280	100	864	1430.3
300	50	864	1408.6
340	24	864	1366.3
380	24	864	1325.2
380*	24	256	1327.0

Table S12: Parameters characterizing the performed MD simulations of [C_5Py][NTf_2]. t_{sim}: total simulation time; N_{IP}: number of ion pairs; ρ: mass density.

T/K	t_{sim}/ns	N_{IP}	ρ/kg m^{-3}
300	100	512	1370.1
320	100	512	1347.7
340	100	512	1326.0
360	100	512	1304.1
380	100	512	1282.9
400	100	512	1262.1

S8 Dissected spin-lattice relaxation rates

In addition to the optimized values obtained by the fitting procedure described in section S4, it is possible to dissect the experimentally measured relaxation rates into the intermolecular and intramolecular relaxation contributions according to Eqs. (1) and (2). A complete overview of the decompositions for all temperatures and nuclei is given on the following pages.

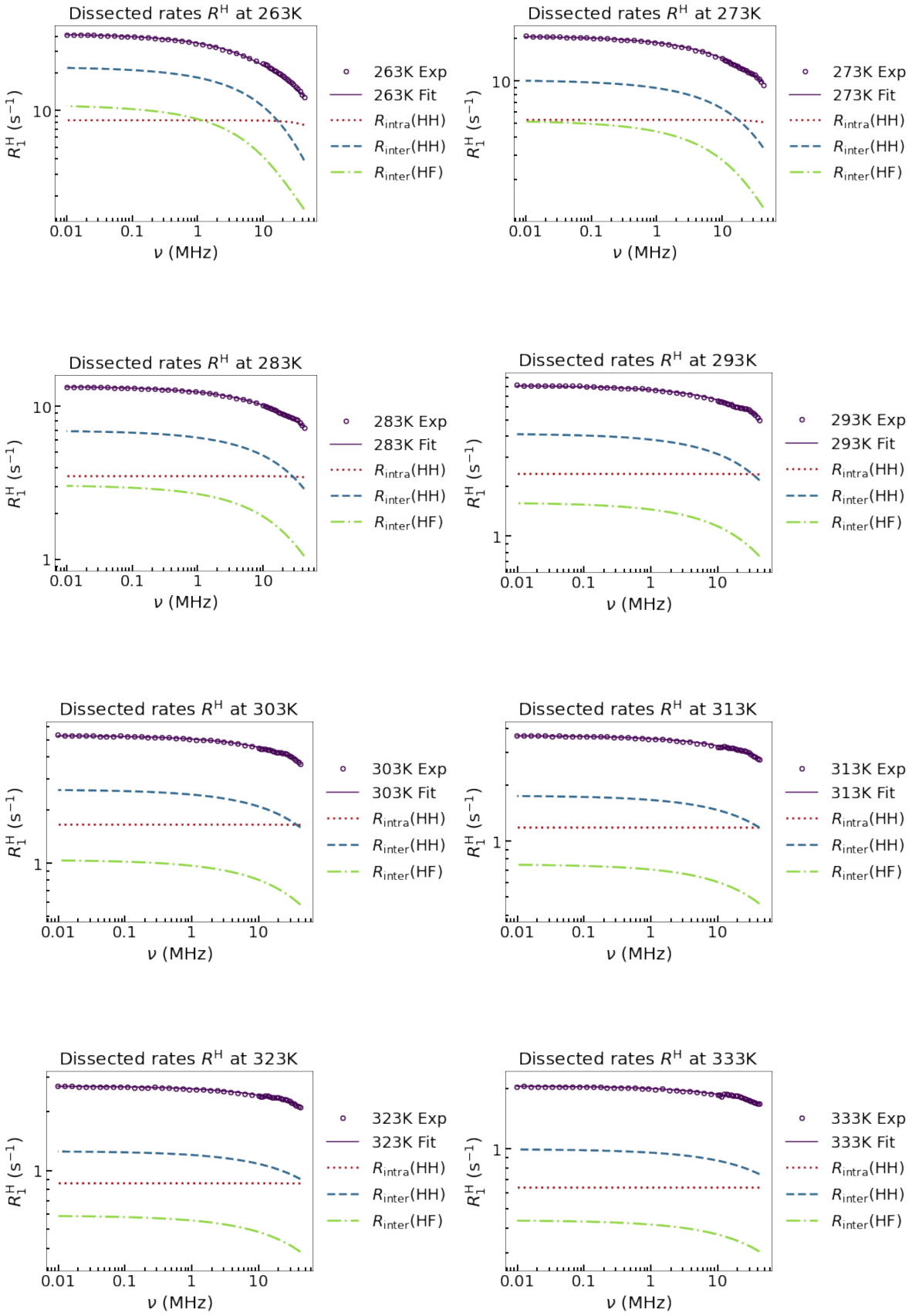

Figure S1: Frequency-dependent NMRD profiles for ^{1}H (cation) in the IL [TEA][NTf$_2$]. Each subplot corresponds to a different temperature. Experimental data are plotted as open circles, while the total fits corresponding to Eqs. (1), (11), and (29) are shown as purple solid lines. The contributions from homonuclear intramolecular relaxation $R_{\mathrm{intra}}(\mathrm{HH})$ are shown as red dotted lines, homonuclear intermolecular contributions $R_{\mathrm{inter}}(\mathrm{HH})$ as blue dashed lines, and heteronuclear intermolecular contributions $R_{\mathrm{inter}}(\mathrm{HF})$ are represented by green dashed dotted lines.

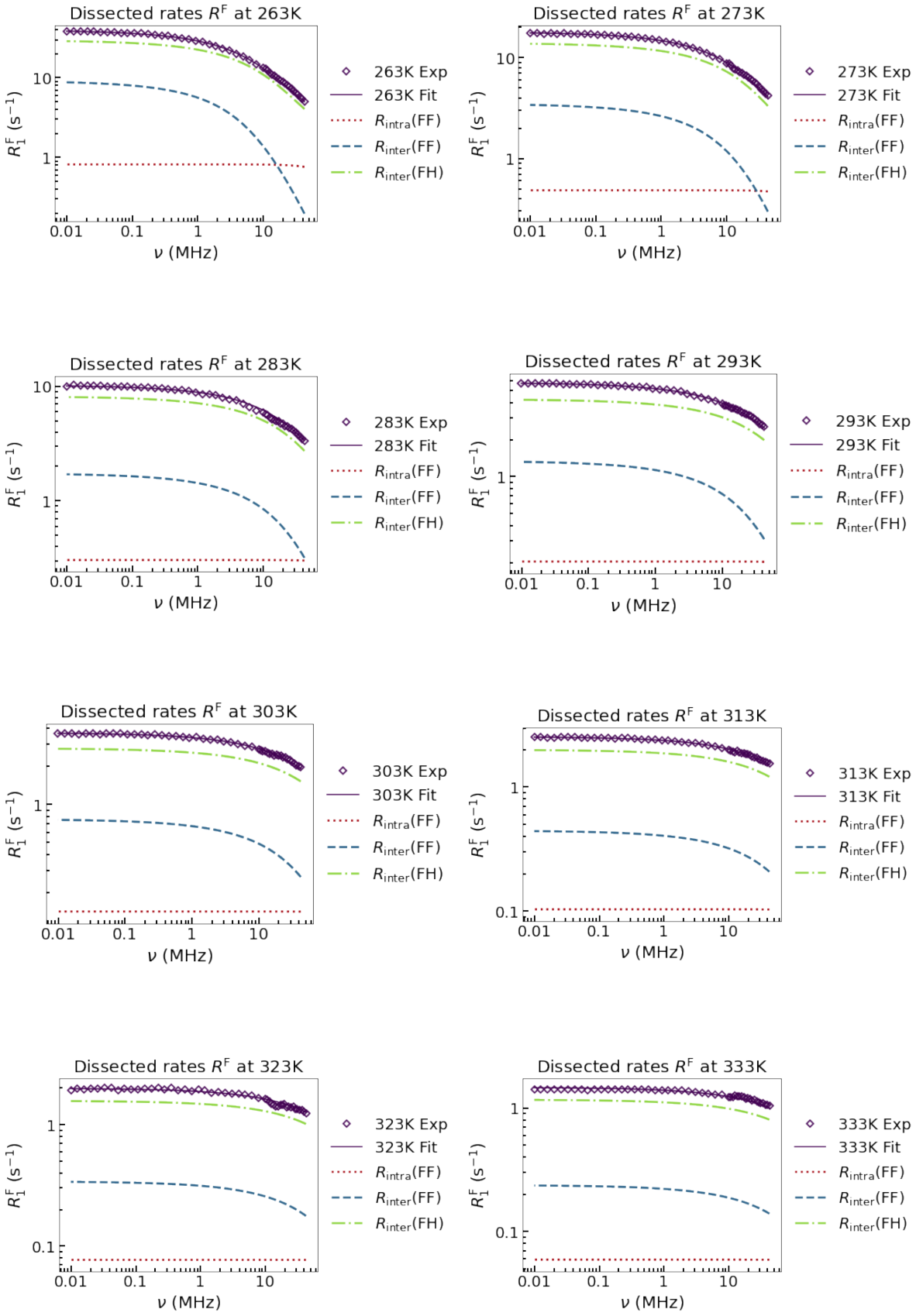

Figure S2: Frequency-dependent NMRD profiles for ^{19}F (anion) in the IL [TEA][NTf_2]. Each subplot corresponds to a different temperature. Experimental data are plotted as open diamonds, while the total fits corresponding to Eqs. (2), (22), and (29) are shown as purple solid lines. The contributions from homonuclear intramolecular relaxation $R_{\mathrm{intra}}(\mathrm{FF})$ are shown as red dotted lines, homonuclear intermolecular contributions $R_{\mathrm{inter}}(\mathrm{FF})$ as blue dashed lines, and heteronuclear intermolecular contributions $R_{\mathrm{inter}}(\mathrm{FH})$ are represented by green dashed dotted lines.

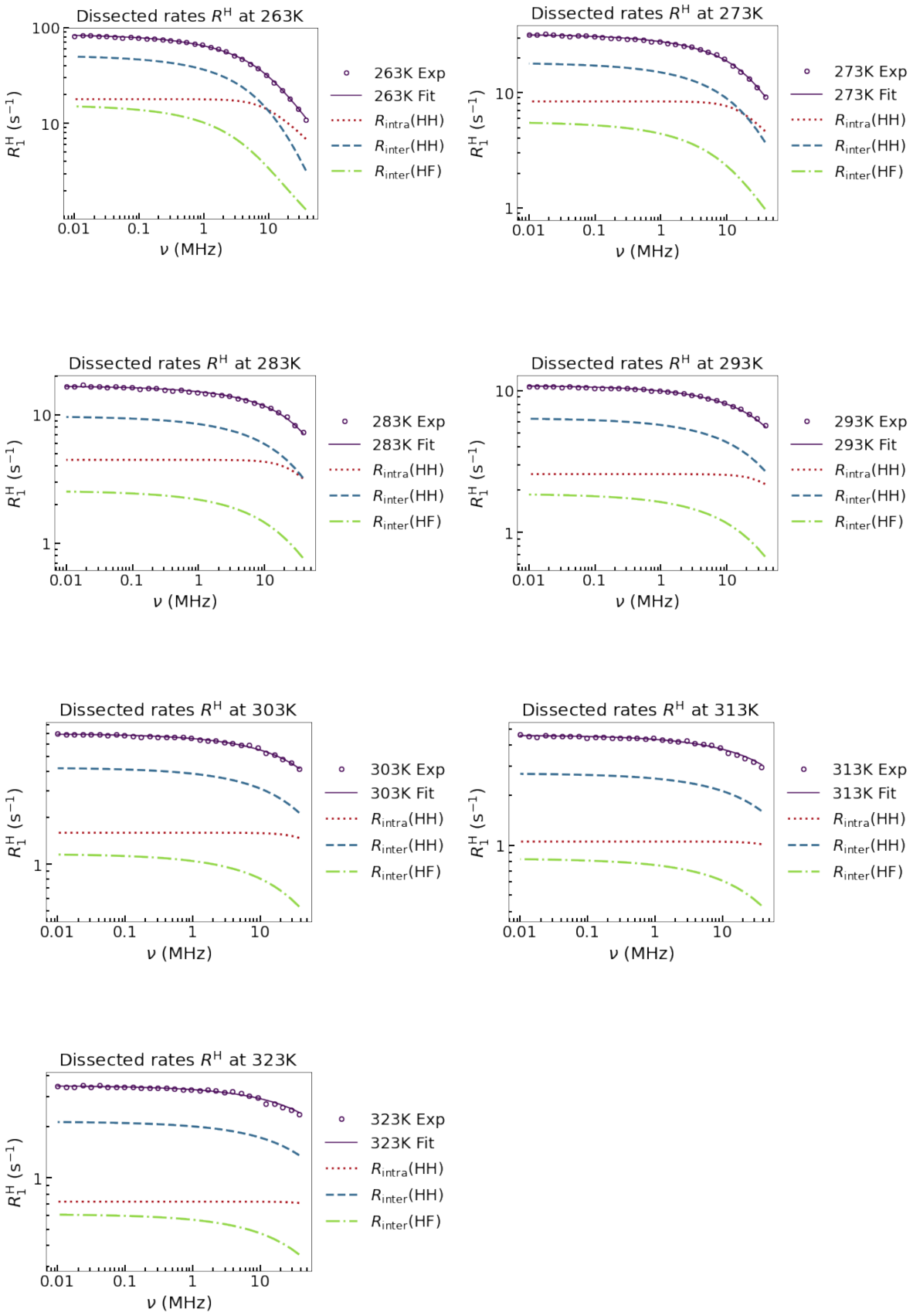

Figure S3: Frequency-dependent NMRD profiles for ^{1}H (cation) in the IL [C_5Py][NTf_2]. Each subplot corresponds to a different temperature. Experimental data are plotted as open circles, while the total fits corresponding to Eqs. (1), (14), and (29) are shown as purple solid lines. The contributions from homonuclear intramolecular relaxation $R_{\mathrm{intra}}(\mathrm{HH})$ are shown as red dotted lines, homonuclear intermolecular contributions $R_{\mathrm{inter}}(\mathrm{HH})$ as blue dashed lines, and heteronuclear intermolecular contributions $R_{\mathrm{inter}}(\mathrm{HF})$ are represented by green dashed dotted lines.

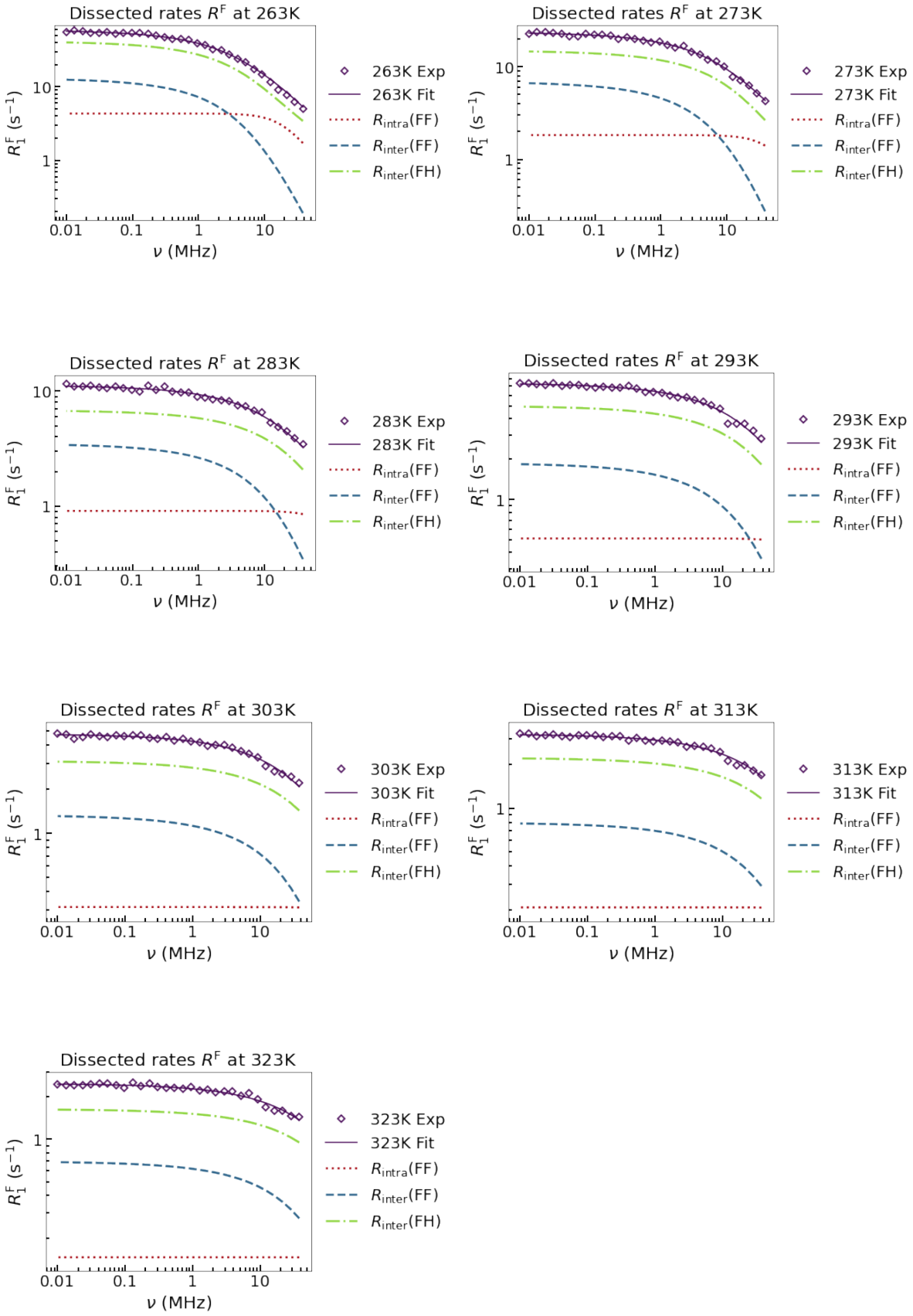

Figure S4: Frequency-dependent NMRD profiles for ^{19}F (anion) in the IL [C_5Py][NTf_2]. Each subplot corresponds to a different temperature. Experimental data are plotted as open diamonds, while the total fits corresponding to Eqs. (2), (22), and (29) are shown as purple solid lines. The contributions from homonuclear intramolecular relaxation $R_{\mathrm{intra}}(\mathrm{FF})$ are shown as red dotted lines, homonuclear intermolecular contributions $R_{\mathrm{inter}}(\mathrm{FF})$ as blue dashed lines, and heteronuclear intermolecular contributions $R_{\mathrm{inter}}(\mathrm{FH})$ are represented by green dashed dotted lines.

S9 Reorientational Correlation Functions

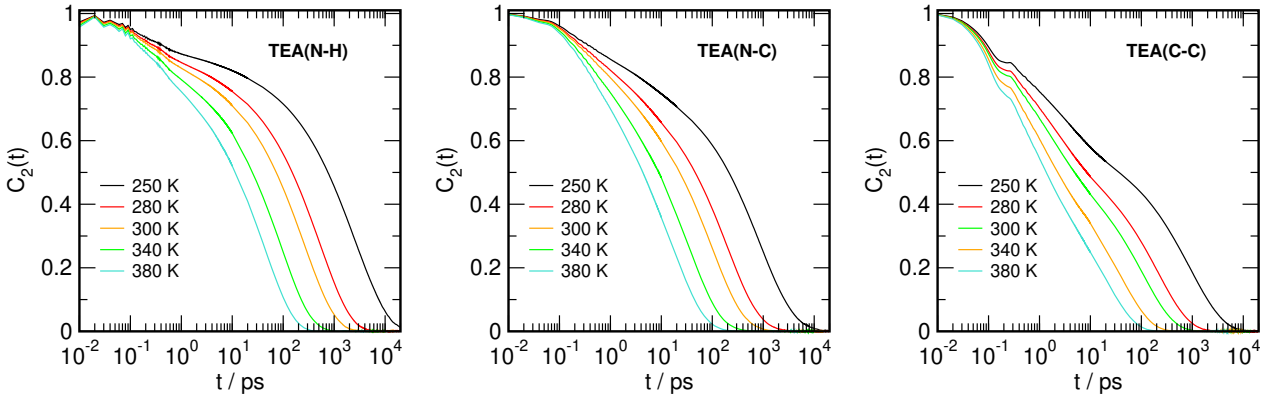

Figure S5: Log-linear plots of the reorientational time correlation functions $C_2(t) = \langle P_2[\vec{u}_{ij}(0) \cdot \vec{u}_{ij}(t)] \rangle$ for three selected intramolecular vectors ij within the [TEA] cation in [TEA][NTF_2] for various temperatures. Here $P_2[\ldots]$ indicates the second Legendre polynomial.

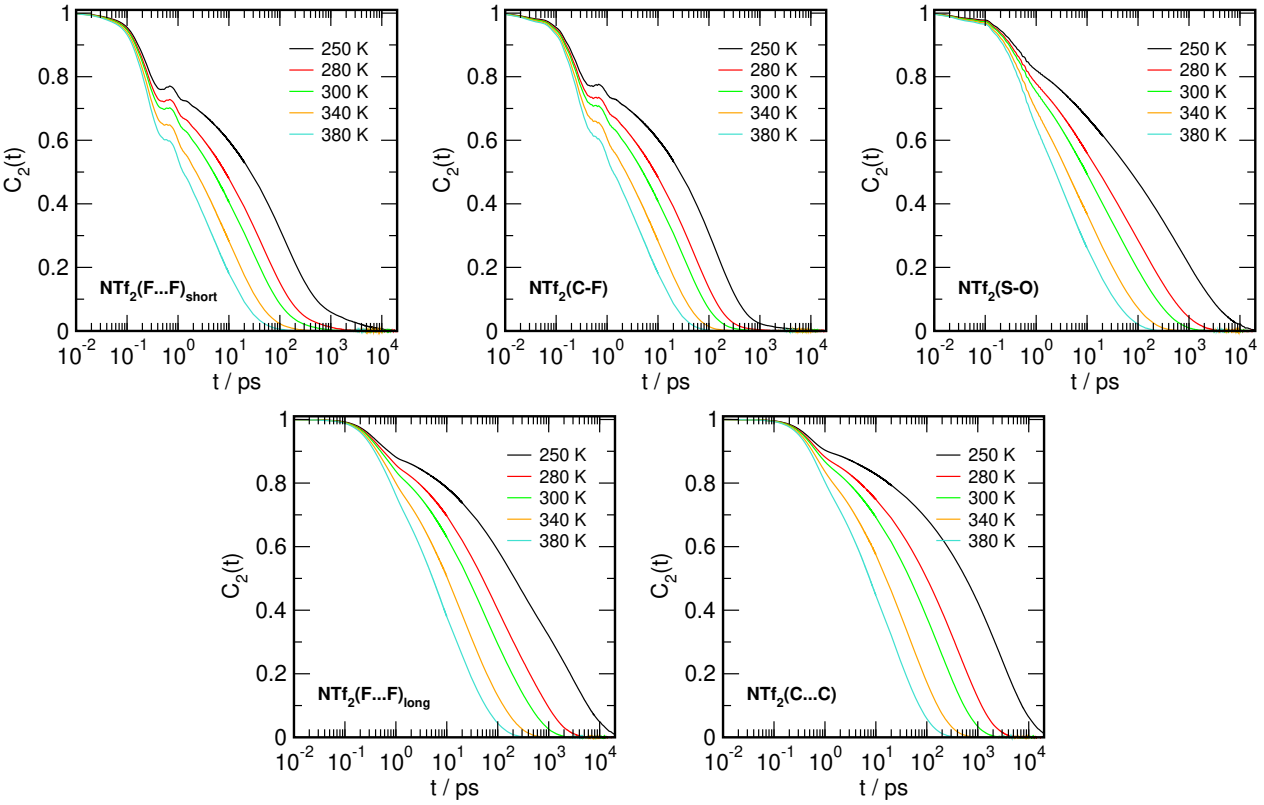

Figure S6: Log-linear plots of the reorientational time correlation functions $C_2(t) = \langle P_2[\vec{u}_{ij}(0) \cdot \vec{u}_{ij}(t)] \rangle$ for five selected intramolecular vectors ij within the [NTF_2] anion in [TEA][NTF_2] for various temperatures. Here $P_2[\ldots]$ indicates the second Legendre polynomial.

References

[1] N. Bloembergen, E. M. Purcell and R. V. Pound, *Phys. Rev.*, 1948, **73**, 679–712.

[2] D. E. Woessner, *The Journal of Chemical Physics*, 1962, **37**, 647–654.

[3] J. Kowalewski, *Nuclear Spin Relaxation in Liquids: Theory, Experiments, and Applications, Second Edition*, Routledge, New York, NY, USA, 2019.

[4] D. E. Woessner, *J. Chem. Phys.*, 1965, **42**, 1855–1859.

[5] H. Versmold, *J. Chem. Phys.*, 1980, **73**, 5310–5313.

[6] H. Versmold, *Ber. Bunsenges. Phys. Chem.*, 1980, **84**, 168–173.

[7] L.-P. Hwang and J. H. Freed, *The Journal of Chemical Physics*, 1975, **63**, 4017–4025.

[8] L. Kruse, A. M. Chiramel Tony, D. Paschek, P. Stange, R. Ludwig and A. Strate, *Journal of Physical Chemistry Letters*, 2024, **15**, 10410–10415.

[9] T. Köddermann, D. Paschek and R. Ludwig, *ChemPhysChem*, 2007, **8**, 2464–2470.

[10] J. Neumann, B. Golub, L.-M. Odebrecht, R. Ludwig and D. Paschek, *J. Chem. Phys.*, 2018, **148**, 193828.

[11] D. Paschek, B. Golub and R. Ludwig, *Phys. Chem. Chem. Phys.*, 2015, **17**, 8431–8440.

[12] B. Golub, D. Ondo, R. Ludwig and D. Paschek, *J. Phys. Chem. Lett.*, 2022, **13**, 3556–3561.

[13] J. Neumann, D. Paschek, A. Strate and R. Ludwig, *J. Phys. Chem. B*, 2021, **125**, 281–286.

[14] S. Páll, M. J. Abraham, C. Kutzner, B. Hess and E. Lindahl, Solving Software Challenges for Exascale, Cham, 2015, pp. 3–27.

[15] S. Pronk, S. Páll, R. Schulz, P. Larsson, P. Bjelkmar, R. Apostolov, M. R. Shirts, J. C. Smith, P. M. Kasson, D. van der Spoel, B. Hess and E. Lindahl, *Bioinformatics*, 2013, **29**, 845–854.

[16] B. Hess, C. Kutzner, D. van der Spoel and E. Lindahl, *J. Chem. Theory Comput.*, 2008, **4**, 435–447.

[17] D. van der Spoel, E. Lindahl, B. Hess, G. Groenhof, A. E. Mark and H. J. C. Berendsen, *J. Comput. Chem.*, 2005, **26**, 1701–1718.

[18] H. J. C. Berendsen, D. van der Spoel and R. van Drunen, *Comput. Phys. Commun.*, 1995, **91**, 43–56.

[19] H. J. C. Berendsen, J. P. M. Postma, W. F. van Gunsteren, A. Di Nola and J. R. Haak, *J. Chem. Pys.*, 1984, **81**, 3684–3690.

[20] S. Nosé, *J. Chem. Pys.*, 1984, **81**, 511–519.

[21] W. G. Hoover, *Phys. Rev. A*, 1985, **31**, 1695–1697.

[22] M. Parrinello and A. Rahman, *Journal of Applied Physics*, 1981, **52**, 7182–7190.

[23] S. Nosé and M. L. Klein, *Molecular Physics*, 1983, **50**, 1055–1076.

[24] J. E. Basconi and M. R. Shirts, *J. Chem. Theory Comput.*, 2013, **9**, 2887–2899.

[25] B. Hess, H. Bekker, H. J. C. Berendsen and J. G. E. M. Fraaije, *J. Comput. Chem.*, 1997, **18**, 1463–1472.

[26] U. Essmann, L. Perera, M. L. Berkowitz, T. Darden, H. Lee and L. G. Pedersen, *J. Chem. Phys.*, 1995, **103**, 8577–8593.